PHILOSOPHICAL TRANSACTIONS OF THE ROYAL SOCIETY A

Phil. Trans. R. Soc. A (2006) **364**, 663–677
doi:10.1098/rsta.2005.1730
Published online 24 January 2006

The generation of mono-energetic electron beams from ultrashort pulse laser–plasma interactions

By S. P. D. Mangles[1], K. Krushelnick[1,*], Z. Najmudin[1], M. S. Wei[1], B. Walton[1], A. Gopal[1], A. E. Dangor[1], S. Fritzler[2], C. D. Murphy[1,3], A. G. R. Thomas[1], W. B. Mori[5], J. Gallacher[4], D. Jaroszynski[4], P. A. Norreys[3] and R. Viskup[4]

[1]*Blackett Laboratory, Imperial College, London SW7 2BZ, UK*
[2]*Laboratoire d'Optique Appliquée, École Nationale Supérieure des Techniques Avancées, École Polytechnique, CNRS, UMR 7639, 91761 Palaiseau, France*
[3]*Central Laser Facility, Rutherford Appleton Laboratory, Chilton, Didcot, Oxon OX11 0QX, UK*
[4]*Department of Physics, University of Strathclyde, Glasgow G4 0NG, UK*
[5]*Department of Physics, University of California, PO Box 951310, 10244 Bunche Hall, Los Angeles, CA 90095-1310, USA*

The physics of the interaction of high-intensity laser pulses with underdense plasma depends not only on the interaction intensity but also on the laser pulse length. We show experimentally that as intensities are increased beyond $10^{20}\,\mathrm{W\,cm^{-2}}$ the peak electron acceleration increases beyond that which can be produced from single stage plasma wave acceleration and it is likely that direct laser acceleration mechanisms begin to play an important role. If, alternatively, the pulse length is reduced such that it approaches the plasma period of a relativistic electron plasma wave, high-power interactions at much lower intensity enable the generation of quasi-mono-energetic beams of relativistic electrons.

Keywords: lasers; plasmas; particle acceleration

1. Introduction

High-power laser technology has advanced significantly over the past several years. It is now possible to perform experiments with high-energy 'Petawatt' ($10^{15}\,\mathrm{W}$) class laser systems at large laser facilities and equally possible to perform high-intensity experiments using ultrashort pulse laser systems (sub 50 fs) which have high repetition rates and which fit into a university scale laboratory (Perry & Mourou 1994). Both of these types of lasers are capable of producing unique states of matter which can have relativistic 'temperatures' (Key *et al.* 1998), ultrastrong magnetic fields (Tatarakis *et al.* 2002) and which

* Author for correspondence (k.krushelnic@ic.ac.uk).

One contribution of 15 to a Discussion Meeting Issue 'Laser-driven particle accelerators: new sources of energetic particles and radiation'.

can produce beams of energetic electrons (Sprangle *et al.* 1988; Nakajima *et al.* 1995; Umstadter *et al.* 1996; Ting *et al.* 1997; Santala *et al.* 2001; Joshi & Katsouleas 2003), ions (Krushelnick *et al.* 1999; Clark *et al.* 2000) and gamma rays (Edwards *et al.* 2002). This has consequently led to significant interest in these systems for technological applications as well as for the examination of fundamental scientific issues.

A particularly exciting application of laser produced plasmas is the potential development of high field, 'compact' electron accelerators (Tajima & Dawson 1979). In recent experiments we have evaluated the use of both a Petawatt class laser and a high repetition rate ultrashort pulse system for relativistic electron acceleration applications. The acceleration mechanism for most previous experiments has been the production of relativistic plasma waves, which can trap and accelerate electrons. Such waves can be produced via instabilities which occur during the interaction (such as the self-modulation instability–self-modulated laser wakefield acceleration (SM-LWFA)). We have found that for interactions in the 'picosecond' pulse-duration regime the electron acceleration mechanism changes from relativistic plasma wave acceleration to direct laser acceleration (DLA) as the intensity is increased. The limiting electron energy for plasma wave acceleration is due to the well known dephasing limit—however, for direct acceleration mechanisms the ultimate limit is not clear. Although the relativistic electron bunches generated from these experiments are highly directional and contain significant amounts of charge, they are emitted with an extremely large energy spread making many of the potentially important applications for electron beams unfeasible with these sources.

However, in recent experiments also described here, we show that for high-power experiments using much shorter pulses (in the tens of femtoseconds regime) it is possible to generate true 'beams' of relativistic electrons which have low divergence and which have a relatively small energy spread (less than 5%; Mangles *et al.* 2004).

This is an extremely important result since only if narrow energy bandwidths are achievable will the full range of applications become possible. The use of plasma acceleration consequently now offers the potential of significantly smaller and cheaper facilities for generating energetic electron beams which, considered along with the current rapid developments in laser technology, could soon allow the construction of university laboratory scale accelerators for use in a wide range of experiments and applications (Faure *et al.* 2004; Geddes *et al.* 2004). For example, table-top narrowband femtosecond X-ray sources and free-electron lasers could become a reality—potentially leading to significant advances in both medicine and material science. It may also be possible to use electron bunches generated in this way for injection into conventional rf accelerators or into subsequent plasma acceleration stages.

2. Laser acceleration of electrons at intensities greater than 10^{20} W cm^{-2}

The recent development of Petawatt class lasers such as that at the Central Laser Facility at the Rutherford Appleton Laboratory in the UK (Vulcan) has allowed experiments to be performed at much higher intensities than previously available. The field amplitude of a laser pulse is often described by the

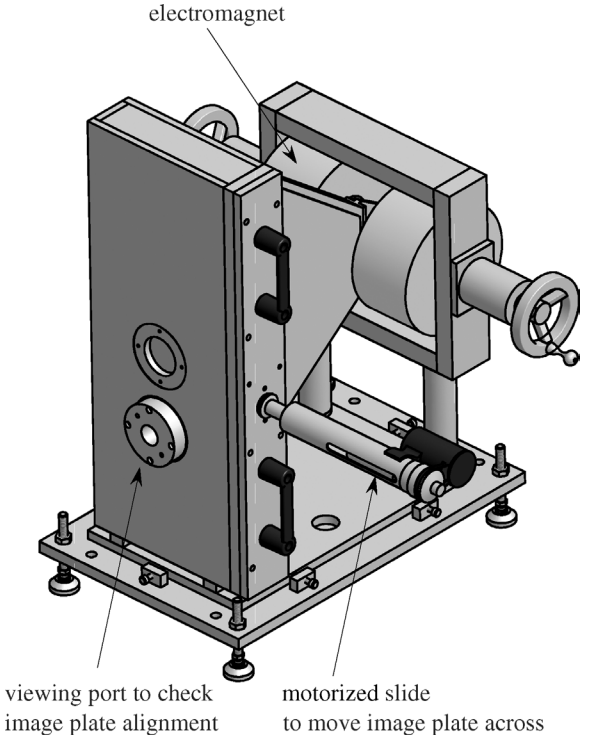

Figure 1. Schematic of electron spectrometer 2: 50.8 mm pole pieces. (Drawing courtesy of B. Fell, CCLRC Rutherford Appleton Laboratory.)

normalized vector potential of the laser field, $a_0 = eA/mc^2$ (A is the vector potential of the laser field and m is the electron mass). a_0 is also the normalized transverse momentum of the electron motion in the laser field. As a_0 approaches 1 the electron motion becomes relativistic. The Vulcan Petawatt facility allows experimental access to regimes where $a_0 \gg 1$ (and in the experiment reported here $a_0 \approx 15$).

During this experiment the laser consistently produced 650 fs duration pulses delivering approximately 180 J on target. These pulses were focused with an $f/3$ off-axis parabolic mirror to produce a focal spot with an intensity FWHM (full width half maximum) of approximately 10 μm, thus generating intensities greater than 3×10^{20} W cm^{-2}.

The gas jet used had a 2 mm diameter supersonic nozzle and could produce plasma electron densities between 5×10^{18} and 2×10^{20} cm^{-3}. The density was controlled by varying the backing pressure behind the valve of the gas jet. The density was determined by measuring the wavelength shift of the forward Raman scattered satellites. Two series of shots were performed in this particular experiment, one with helium and the other with deuterium. Since He^{2+} and D^+ have the same charge to mass ratio there should be little qualitative difference in the two datasets (which indeed was observed to be the case).

The electrons accelerated along the axis of laser propagation were measured using a high field magnetic spectrometer (figure 1). The electrons exited the highly shielded main vacuum chamber through a small (25 mm) diameter tube to

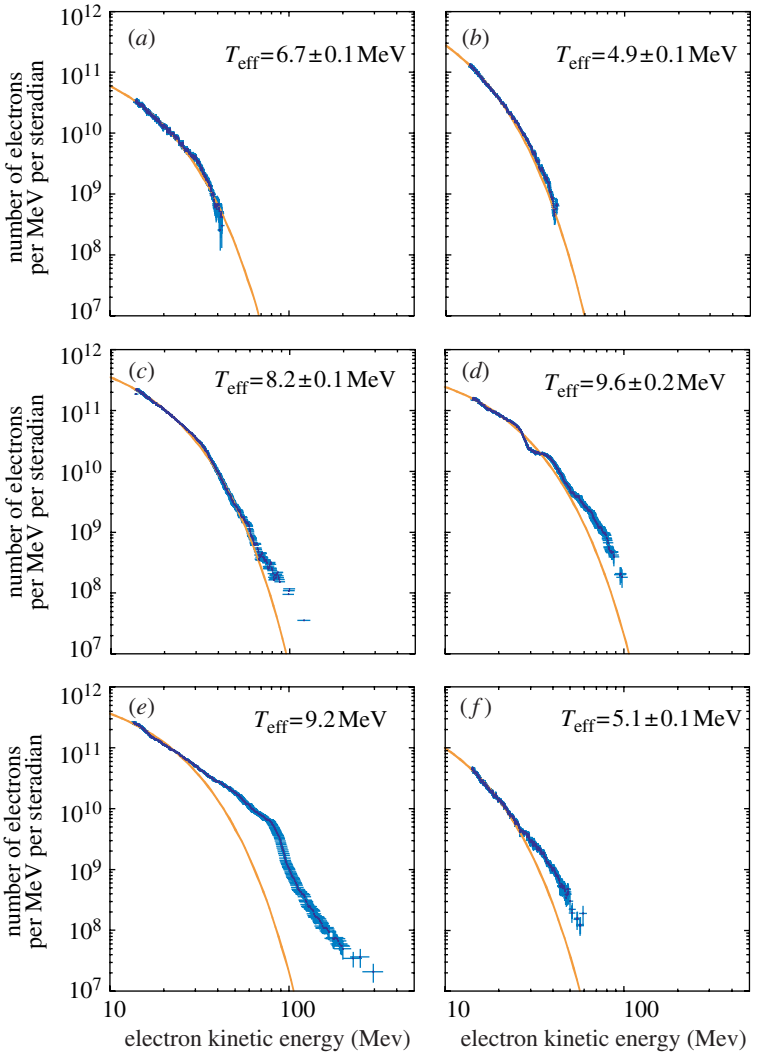

Figure 2. Electron energy spectrum over a range of electron densities. (*a*) $n_{\mathrm{e}}=138\pm3\times10^{18}\ \mathrm{cm}^{-3}$; $E=165$ J, $\tau=690$ fs, (*b*) $n_{\mathrm{e}}=83\pm3\times10^{18}\ \mathrm{cm}^{-3}$; $E=165$ J, $\tau=690$ fs, (*c*) $n_{\mathrm{e}}=14\pm2\times10^{18}\ \mathrm{cm}^{-3}$; $E=180$ J, $\tau=640$ fs, (*d*) $n_{\mathrm{e}}=9.2\pm1.2\times10^{18}\ \mathrm{cm}^{-3}$; $E=165$ J, $\tau=640$ fs, (*e*) $n_{\mathrm{e}}=7.7\pm0.7\times10^{18}\ \mathrm{cm}^{-3}$; $E=160$ J, $\tau=690$ fs and (*f*) $n_{\mathrm{e}}=5.4\pm0.6\times10^{18}\ \mathrm{cm}^{-3}$; $E=165$ J, $\tau=690$ fs.

a secondary vacuum vessel—which helps to reduce the level of background signal from low-energy X-rays and scattered electrons. The entrance to the spectrometer was a 5 mm diameter aperture which ensured good energy resolution for the measurement of the electrons. The specially designed vacuum chamber allowed the electron beam to pass between the pole pieces of an electromagnet (figure 1) that deflected the electrons off-axis. The correspondence between electron energy and deflection from the axis was determined by using a charged particle tracking code.

In these experiments, electrons were detected using an image plate, which is a re-usable film sensitive to ionizing radiation. Two sections of image plate were

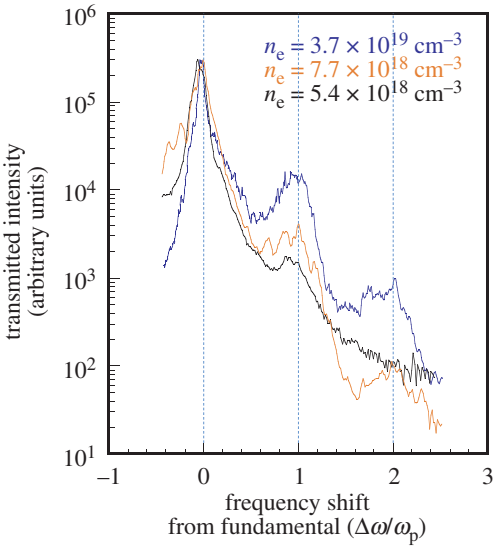

Figure 3. Forward scattered spectrum at various electron densities. The frequency is shown as a shift from the fundamental, normalized to the plasma frequency for each density.

used, one to measure the electron signal below axis, and another to measure the background signal above the axis. Since the background is due to X-rays from the interaction itself or from bremsstrahlung radiation emitted by the electrons as they pass through material before the detector plane, it was assumed that the background was symmetric above and below the axis.

The relationship between image plate signal intensity and energy deposited in the plate is close to linear. This has been confirmed by previous studies (Gales & Bentley 2004). The direct relationship between the number of electrons and the signal was calculated by placing a diode array directly behind the image plates. The ion implanted diodes used have an absolutely calibrated response to the number of electrons incident and by calculating the energy lost by the electrons as they travel through the plate before reaching the diodes it is possible to cross-calibrate the diode and image plate signals.

The image plate data exhibits a much larger dynamic range than the diodes and the 'image' nature of the data also allows much better noise discrimination. The resolution of the image plates, although not as high as X-ray film is significantly better than the diode array. The combination of the resolution and size of the image plates (each is 250 mm long) allows a reasonably broad energy range (for example, 10–250 MeV) to be measured in a single shot.

The laser–plasma interaction was also diagnosed by measuring the transmitted spectrum of the laser. A portion of the transmitted beam was collimated and transported out of the vacuum chamber to a pair of near-infrared spectrometers; CCD cameras recorded the spectra on each shot at two different dispersions.

Figure 2 shows a number of electron energy spectra obtained from shots with helium gas. These shots have been selected to show the trend observed as the density of the gas jet was decreased. Electrons were accelerated to relativistic

energies at all densities. At high densities ($n_e > 10^{20}\,\mathrm{cm}^{-3}$) the electron energy spectrum can be characterized by an effective temperature (figure 2*a*), that is the distribution of accelerated electrons f, at energy E was given by $f(E) \propto \exp(-E/T_{\mathrm{eff}})$. As the density was decreased (figure 2*b–d*) the maximum energy observed increased, along with T_{eff}. The spectrum also begins to take on a non-Maxwellian form. At $n_e = (0.7 \pm 0.1) \times 10^{19}\,\mathrm{cm}^{-3}$ (figure 2*e*) the acceleration is significantly enhanced, and the energy observed was up to about 300 MeV. The maximum is, in this case, limited by the noise level on the image plate. As the density was decreased further (figure 2*f*) the acceleration was observed to be less effective and the spectrum regains its effective temperature form.

The acceleration was observed to vary with electron density for both helium and deuterium shots. The characteristic electron energy (this was chosen to be when the ratio of signal to noise is 10) was observed to vary strongly with density exhibiting an apparent maximum around $1 \times 10^{19}\,\mathrm{cm}^{-3}$. The shots taken with deuterium gas produced similar spectra, and show the same variation with density, although the 'optimum density' is shifted slightly to $(1.4 \pm 0.2) \times 10^{19}\,\mathrm{cm}^{-3}$.

Figure 3 shows the relationship between the forward Raman scattering (FRS) spectrum and the electron density. The production of high-energy electrons and FRS are uncorrelated. This is in marked difference to previous lower intensity experiments (Modena *et al.* 1995; Santala *et al.* 2001) and indicates that the acceleration mechanism cannot be SM-LWFA since the generation of forward scattered satellites is direct evidence of the production of a relativistic plasma wakefield during the interaction.

A previous study by Gahn *et al.* (1999), with 200 fs, 0.25 J pulses showed enhanced acceleration at an electron density of $2 \times 10^{20}\,\mathrm{cm}^{-3}$. In that experiment there was evidence that electron acceleration is strongly correlated with channel formation. Simulations (Pukhov *et al.* 1999; Pukhov 2003) indicated that when the betatron motion of an electron in a self-generated magnetic field or in the electric field of an evacuated plasma channel is resonant with the relativistic motion of particles in the laser field, electrons can pick up energy directly from the laser pulse (DLA). This is similar to an inverse free-electron laser mechanism and can occur efficiently when the laser power becomes significantly greater than the critical power for relativistic self-focusing.

However, the divergence of the electron beam suggested from these previous lower intensity experiments and simulations is large. With the much smaller divergence electron beam observed in the Vulcan Petawatt experiments (see figure 4 for typical measurements of the electron beam divergence) the mechanism of DLA seems to be more complex and may involve a stochastic 'de-phasing' process (Meyer-ter-Vehn & Sheng 1999; Mangles *et al.* 2005) resulting from the combined effect of the laser electric field with the electrostatic fields due to charge displacement occurring during the intense laser–plasma interaction.

3. Mono-energetic beam production using ultrashort pulses

We have also performed electron acceleration experiments using a second laser system, the high-power ultrashort pulse Titanium:Sapphire Astra laser system at

the Central Laser Facility of the Rutherford Appleton Laboratory. The laser pulses ($\lambda = 800$ nm, $E = 350$ mJ, $\tau = 40$ fs) were focused with an $f/16.7$ off-axis parabolic mirror onto the edge of a 2 mm long supersonic jet of helium gas to produce intensities of the order of 1.3×10^{18} W cm^{-2} (see figure 5). The electron density (n_e) as a function of backing pressure on the gas jet was again determined by measuring the frequency shift ($\Delta\omega = \omega_{pe}$ where ω_{pe} is the electron plasma frequency) of satellite wavelengths generated by FRS in the transmitted light. The plasma density was observed to vary linearly with backing pressure within the range $n_e = 3 \times 10^{18}$–5×10^{19} cm^{-3}. In this density range the wavelength of relativistic plasma waves produced (i.e. $\lambda_p = 2\pi c\omega_{pe}$) is between 0.4 and 1.6 times the laser pulse length ($c\tau_L$). For laser pulses which are less than the plasma wavelength, relativistic plasma waves can be generated 'resonantly' in the wake of the pulse—while in the regime in which the laser pulse length is longer than the plasma wavelength, high-intensity interactions are required to drive an instability in which the plasma waves are produced via 'self-modulation' of the laser pulse envelope at the plasma frequency.

In the work described here, it is possible that at high density self-modulation can play a role in plasma wave generation. However, in most cases in our experiments the interaction is quite close to being in the 'resonant' regime. In these experiments, the intensity is sufficiently high that plasma waves are driven so that they grow until 'wavebreaking' occurs. This is a phenomenon which takes place at very large amplitudes such that the wave motion becomes so nonlinear that wave energy is transferred directly into particle energy and the plasma wave loses coherence. Electrons which reach relativistic energies from wavebreaking of a plasma wave can be 'injected' into an adjacent plasma wave where they can pick up even more energy (the 'cold' wavebreaking electric-field amplitude for electron plasma waves is given by, $E = m_e c\omega_{pe}/e$). Note that in a regime between SM-LWFA and the standard 'resonant' LWFA lies the F-LWFA (*forced* laser wakefield accelerator; Malka *et al.* 2002), where a short pulse is used which is only slightly longer than the resonant pulse length. This pulse is consequently focused and compressed by the wave to produce large amplitude plasma waves which can break.

In the experiment described here, the electron energy spectrum was measured using an on-axis magnetic spectrometer similar to that used in the Petawatt experiments. The electrons were also simultaneously measured with the high-resolution image plate detectors as well as using a much lower resolution array of diodes. The spectrometer magnet, image plates and diodes were set up to measure the spectrum over a wide energy range in a single shot.

Other diagnostics used in this case included the simultaneous measurement of the transmitted laser spectrum and transverse optical probing of the interaction with a frequency doubled laser probe beam. This was used to produce images of the plasma via shadowgraphy, and was independently timed so it could also be used to measure pre-pulse effects and plasma channel formation.

Electron acceleration was observed over a range of electron densities. With the plasma density below 7.3×10^{18} cm^{-3} no energetic electrons were observed (this corresponds to $c\tau_L < \lambda_p$). In this regime, the rate of the plasma wave growth is too low to reach wavebreaking amplitudes.

As the density was increased above 7×10^{18} cm^{-3}, very high-energy electrons were suddenly produced with the most energetic electrons reaching up to

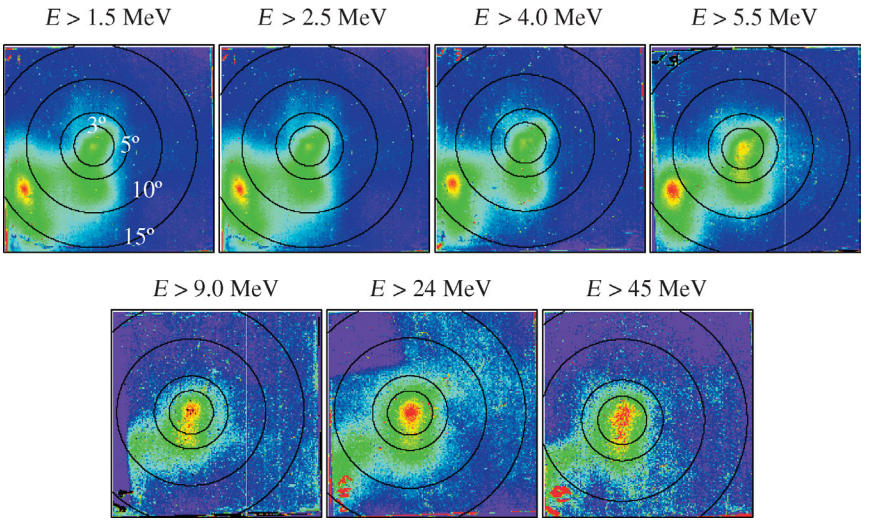

Figure 4. Electron beam divergence measurement at $n_e = 7.5 \times 10^{18}$ cm^{-3}. Contours at 3, 5, 10 and 15° centred on the electron beam axis are shown. Each image is shown normalized to the peak signal for that energy bin.

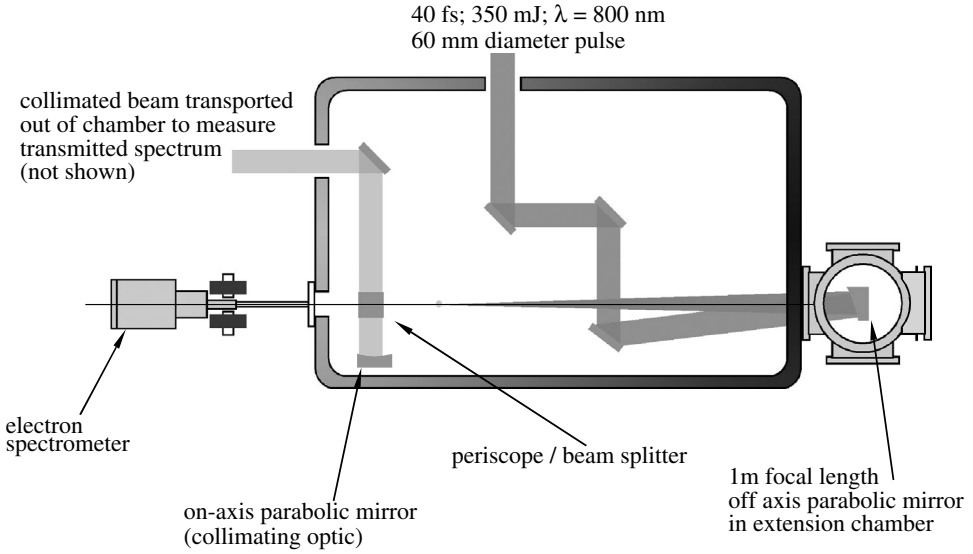

Figure 5. Experimental set-up for the 40 fs 350–500 mJ experiments.

100 MeV. The output beam divergence was also measured and was found to be less than 5°. However, the most interesting aspect of these spectra is that, in this regime, the electron energies were exceptionally non-Maxwellian and, indeed, generally consisted of one or more narrow spiky features—each of which could have an energy bandwidth of less than 20% (see figure 6). This is in contrast to the energy spectra of previous laser acceleration experiments in which 100% energy spreads are observed. As the density was increased in our experiments, the peak energy of the observed electrons was observed to decrease and the

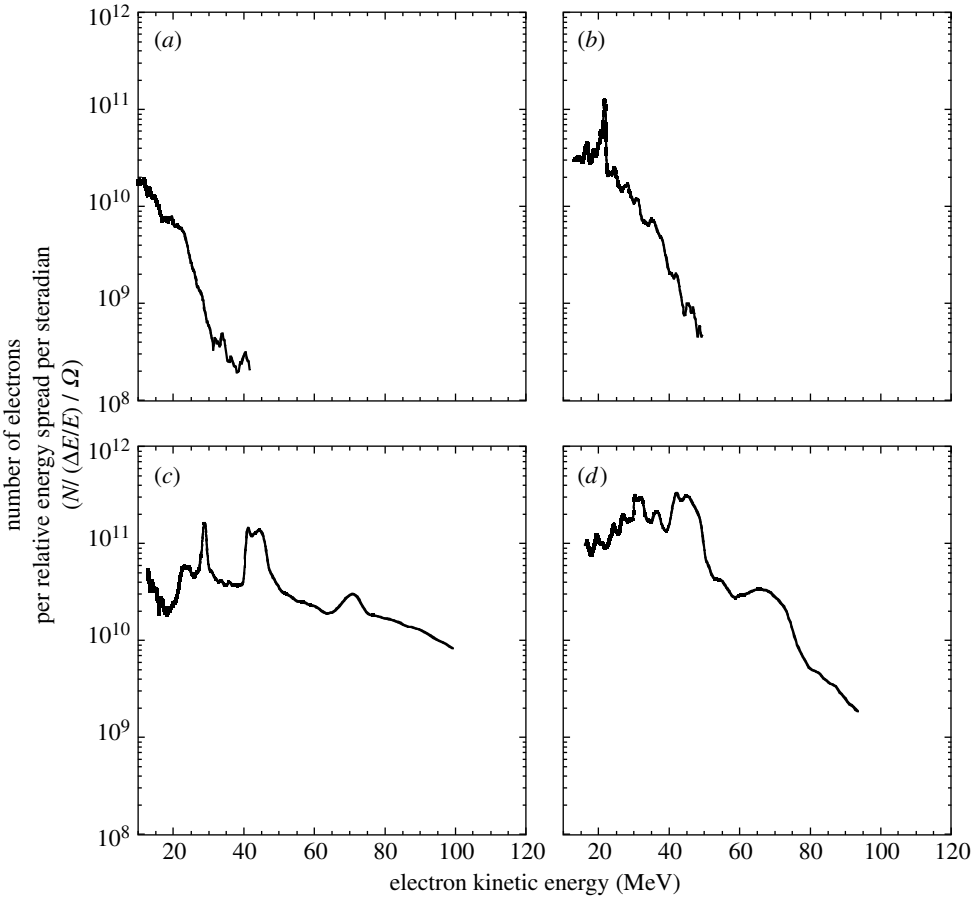

Figure 6. Observed electron spectrum at a various plasma densities. (*a*) $n_e = 5\times10^{19}\,\mathrm{cm}^{-3}$, (*b*) $n_e = 3\times10^{19}\,\mathrm{cm}^{-3}$, (*c*) $n_e = 1.8\times10^{19}\,\mathrm{cm}^{-3}$ and (*d*) $n_e = 1.6\times10^{19}\,\mathrm{cm}^{-3}$. Laser pulse parameters: $E \approx 350$ mJ, $\tau \approx 40$ fs, $I \approx 1.5\times10^{18}\,\mathrm{W\,cm}^{-2}$.

spectra begin to assume a broad Maxwellian shape which was characteristic of previous experiments in the SM-LWFA regime. The total amount of charge in the beam above 20 MeV was also reduced (figure 7).

The likely explanation for the difference observed in these spectra is due to the timing of the 'injection' of electrons into the relativistic plasma wave. It appears that as the plasma wave reaches an amplitude which is just sufficient for wavebreaking only a few electrons are able to 'fall' into the accelerating portion of the adjacent waves in the wake, and so these electrons all see an almost identical acceleration gradient. Since successive waves in the wakefield are of different amplitude (i.e. they have differing accelerating gradients) different trapped bunches will be accelerated to different energies.

In addition, because of the low density these electron bunches are not 'dephased' since the propagation distance is only about 1 mm (or the length of the gas jet plasma). The dephasing distance is the length over which an electron outruns the plasma wave—and begins to be de-accelerated by the wave, and is given as $L_d = 2\pi c\omega^2/\omega_{pe}^3$. For our experiments, the conditions which showed the

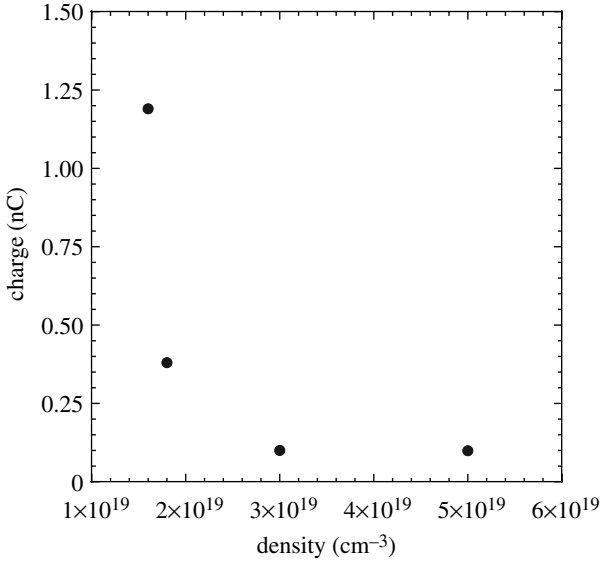

Figure 7. Total charge measured in the spectrometer between 20 and 100 MeV as a function of plasma density for the spectra shown in figure 6.

clearest, most reproducible evidence of these electron beams were those in which the de-phasing length, the gas jet length and the confocal parameter of the laser beam are all roughly 1 mm.

In contrast at higher densities the de-phasing distance is much shorter than the interaction distance and so a 'randomized' or quasi-Maxwellian distribution of electrons would emerge from the plasma, with a more significant low-energy component.

In the final set of experiments the energy of the laser pulse was increased to a maximum of about 600 mJ. These experiments showed that for the plasma densities previously used to obtain 'bumpy' spectra in the lower energy situations, now quite 'mono-energetic' spectra could be observed—with less than a doubling in the laser energy. Several representative spectra are shown in figures 8 and 9 for two different densities. It is clear that at this density single 'mono-energetic' spikes in the spectrum are a common feature. However, since the laser pulse energy, focal spot size/shape and pulse duration varied from shot to shot it is difficult to quantify precisely the shot-to-shot fluctuations in the electron beam parameters with respect to the laser parameters. The precise energy of the peak (or peaks), the total charge in the peak, the dark current component, the electron beam pointing as well as the energy spread of the pulse were observed to vary—and such variations were more significant than the corresponding variations in the properties of the initial laser pulse. Indeed, electron beams were not always observed for shots having the same nominal laser conditions. It is of particular importance to determine the precise source of these fluctuations in these electron beams which will allow this behaviour to be reduced.

Such effects may be entirely the result of, for example, electron beam pointing changes due to laser 'hosing' effects (Najmudin *et al.* 2003). It is also possible that operation with a higher intensity laser pulse or within a preformed density

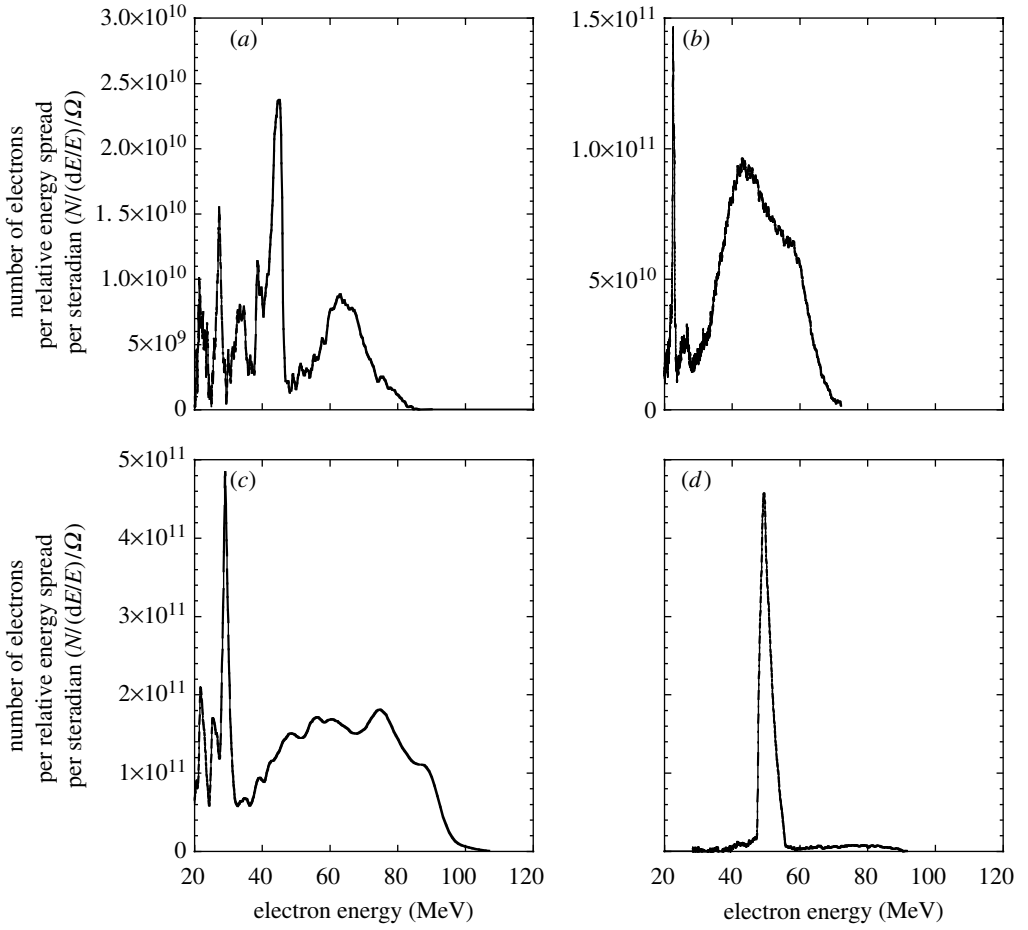

Figure 8. Electron energy spectrum at various plasma densities. Note the different vertical scales. (*a*) $n_e = 1.1 \times 10^{19}$ cm^{-3}. Laser energy = 445 mJ. (*b*) $n_e = 1.3 \times 10^{19}$ cm^{-3}. Laser energy = 600 mJ. (*c*) $n_e = 1.3 \times 10^{19}$ cm^{-3}. Laser energy = 470 mJ. (*d*) $n_e = 1.3 \times 10^{19}$ cm^{-3}. Laser energy = 600 mJ.

channel will enable a more stable regime for the production of these mono-energetic electron beams.

Two-dimensional particle-in-cell simulations of the interaction were performed using the code OSIRIS (Fonseca *et al.* 2002) and it was found that for relatively low plasma densities when the plasma waves grow to an amplitude such that they are observed to break, a group of electrons is injected at a particular phase position in the plasma wave and this group of electrons can be accelerated relatively uniformly. As the laser pulse front begins to steepen, the wakefield amplitude grows and the electron energies increase until the pulse reaches its maximum peak intensity. At this point the electron energies are clearly 'bunched' at a particular energy. After this time the average electron energies begin to drop and the distribution of energies is randomized—since the propagation distance is beyond the dephasing length for this interaction.

The diminished energies can also caused by the 'erosion' of the pulse leading edge, coupled with a nonlinear lengthening of the plasma wavelength in the wake

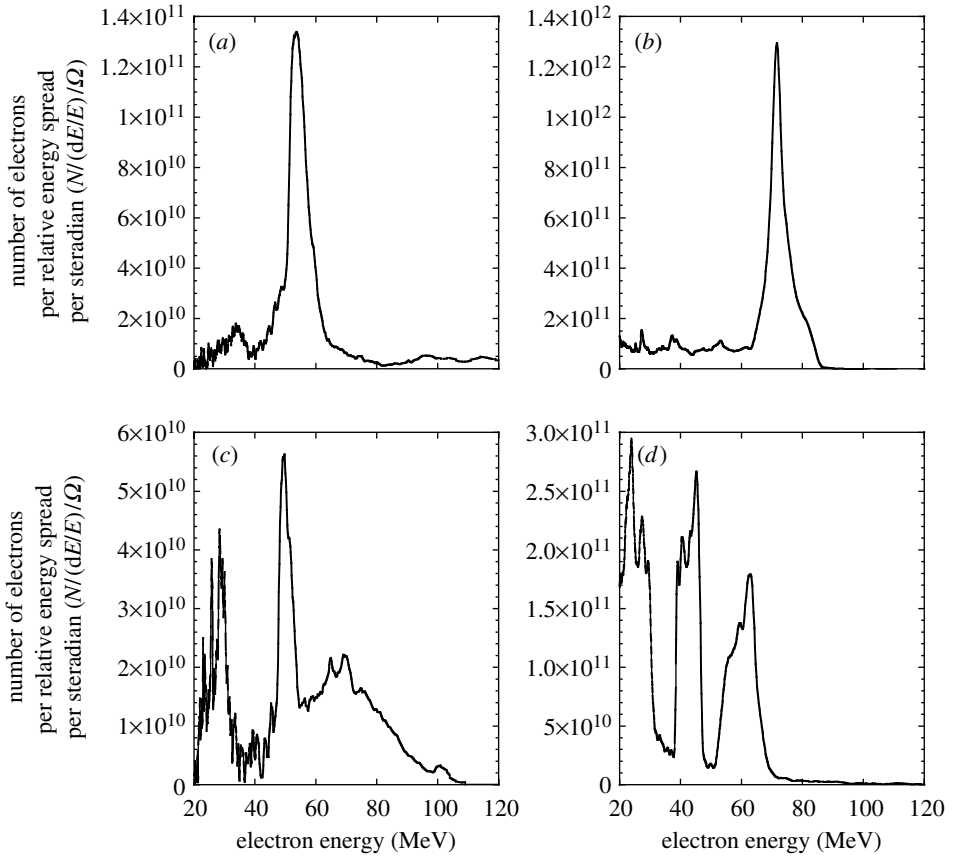

Figure 9. Electron energy spectrum at various plasma densities. Note the different vertical scales. (*a*) $n_e = 1.5 \times 10^{19}\,\mathrm{cm}^{-3}$. Laser energy = 470 mJ. (*b*) $n_e = 1.7 \times 10^{19}\,\mathrm{cm}^{-3}$. Laser energy = 480 mJ. (*c*) $n_e = 1.8 \times 10^{19}\,\mathrm{cm}^{-3}$. Laser energy = 495 mJ. (*d*) $n_e = 1.8 \times 10^{19}\,\mathrm{cm}^{-3}$. Laser energy = 430 mJ.

which may slow the electrons. This process continues so that the bunch again enters a region of accelerating field and the energies increase once more. When the wake reaches its highest amplitude the trapped electrons are completely dephased with respect to the plasma wave.

It is clear from simulations that in our experiments the 'bunches' of electrons are produced due to wavebreaking in the immediate vicinity of the laser pulse. These electrons are then accelerated through the entire length of the plasma—which is shorter than the dephasing distance. Consequently, the bunch of electrons can remain relatively mono-energetic after leaving the plasma. The requirements for this regime are that the plasma density has to be high enough so that wavebreaking is easily achieved—but low enough so that the electron bunches produced are not de-phased before they leave the plasma.

As the density in the simulations is varied (figure 10) it is clear that self focusing and 'pulse compression' effects occur in all cases—but in high-density situations these effects can happen rapidly (in a time inversely proportional to density) such that instabilities result and any bunches of electrons which are produced are quickly de-phased before leaving the plasma.

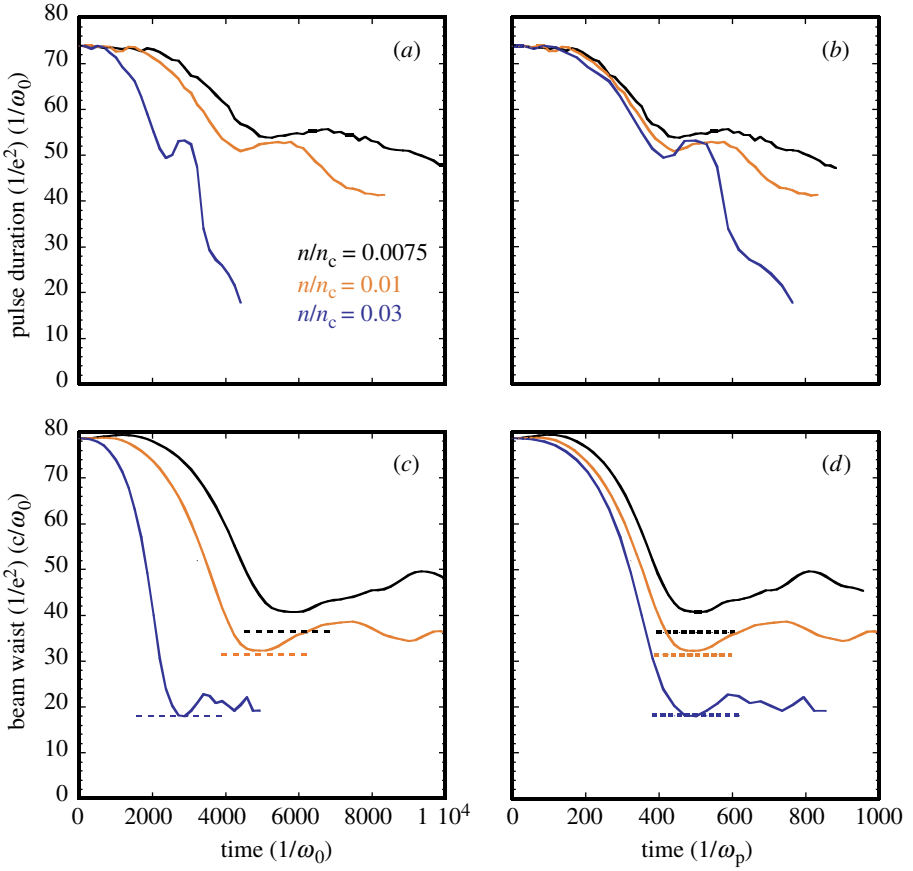

Figure 10. Evolution of the laser pulse during simulations at different densities. (*a*) On-axis laser pulse duration ($1/e^2$ half width) as a function of time ($1/\omega_0$) and (*b*) the number of plasma periods ($1/\omega_p$). (*c*) Average laser waist ($1/e^2$ half width) as a function of simulation time ($1/\omega_0$) and (*d*) the number of plasma periods ($1/\omega_p$). The quantity $\pi c/\omega_p$ is indicated for each density on (*c*) and (*b*) shots are taken from the same series.

4. Conclusions

In summary, experiments on the Vulcan Petawatt facility have successfully accelerated electrons up a maximum energy up to about 300 MeV with low divergence. This is the highest energy observed from any laser–plasma interaction to date. It appears that at such intensities the mechanism for accelerating electrons is no longer the SM-LWFA regime (Modena *et al.* 1995) but rather a form of DLA.

We have also demonstrated that the Astra laser can be used to produce relativistic bunches of electrons with energies beyond 100 MeV. Accelerated electrons are not observed at low density—but at a particular minimum density 'mono-energetic' electron beams can be clearly observed in the spectrum. As the plasma density is increased still further such structures are randomized by the dephasing of the accelerated electrons with the plasma waves and an energy spread of 100% is observed.

The observation that mono-energetic electron beams can be produced using only a laser-produced plasma suggests that such sources hold great promise for future development of table top particle accelerators and that a wide range of applications may soon become possible.

The authors acknowledge the assistance of the staff of the Central Laser Facility of the Rutherford Appleton Laboratory in the execution of this work as well as the support of the UK Engineering and Physical Sciences Research Council (EPSRC). We gratefully acknowledge the OSIRIS consortium which consists of UCLA/IST(Portugal)/USC for the use of OSIRIS.

References

Clark, E. L. *et al.* 2000 Measurements of energetic proton transport through magnetized plasma from intense laser interactions with solids. *Phys. Rev. Lett.* **84**, 670–673. (doi:10.1103/PhysRevLett.84.670)

Edwards, R. D. *et al.* 2002 Characterization of a gamma-ray source based on a laser-plasma accelerator with applications to radiography. *Appl. Phys. Lett.* **80**, 2129–2131. (doi:10.1063/1.1464221)

Faure, J., Glinec, Y., Pukhov, A., Kiselev, S., Gordienko, S., Lefebvre, E., Rousseau, J.-P., Burgy, F. & Malka, V. 2004 A laser-plasma accelerator producing monoenergetic electron beams. *Nature* **431**, 541–544. (doi:10.1038/nature02963)

Fonseca, R. A. *et al.* OSIRIS: a three-dimensional, fully relativistic particle in cell code for modeling plasma based accelerators. Lecture Notes in Computer Science **2331**, p. 342.

Gahn, C., Tsakiris, G. D., Pukhov, A., Meyer-ter-Vehn, J., Pretzler, G., Thirolf, P., Habs, D. & Witte, K. J. 1999 Multi-MeV electron beam generation by direct laser acceleration in high-density plasma channels. *Phys. Rev. Lett.* **83**, 4772–4775. (doi:10.1103/PhysRevLett.83.4772)

Gales, S. G. & Bentley, C. D. 2004 Image plates as X-ray detectors in plasma physics experiments. *Rev. Sci. Instrum.* **75**, 4001–4003. (doi:10.1063/1.1789256)

Geddes, C. G. R., Toth, C., van Tilborg, J., Esarey, E., Schroeder, C. B., Bruhwiler, D., Nieter, C., Cary, J. & Leemans, W. P. 2004 High-quality electron beams from a laser wakefield accelerator using plasma-channel guiding. *Nature* **431**, 538–541. (doi:10.1038/nature02900)

Joshi, C. & Katsouleas, T. 2003 Plasma accelerators at the energy frontier and on tabletops. *Phys. Today* **56**, 47–53.

Key, M. H. *et al.* 1998 Hot electron production and heating by hot electrons in fast ignitor research. *Phys. Plasmas* **5**, 1966–1972. (doi:10.1063/1.872867)

Krushelnick, K., Clark, E. L., Najmudin, Z., Salvati, M., Santala, M. I. K., Tatarakis, M. & Dangor, A. E. 1999 Multi-MeV ion production from high-intensity laser interactions with underdense plasmas. *Phys. Rev. Lett.* **83**, 737–740. (doi:10.1103/PhysRevLett.83.737)

Malka, V. *et al.* 2002 Electron acceleration by a wake field forced by an intense ultrashort laser pulse. *Science* **298**, 1596–1600. (doi:10.1126/science.1076782)

Mangles, S. P. D. *et al.* 2004 Monoenergetic beams of relativistic electrons from intense laser–plasma interactions. *Nature* **431**, 535–538. (doi:10.1038/nature02939)

Mangles, S. P. D. *et al.* 2005 Electron acceleration in cavitated channels formed by a petawatt laser in low-density plasma. *Phys. Rev. Lett.* **94**, 245 001. (doi:10.1103/PhysRevLett.94.245001)

Meyer-ter-Vehn, J. & Sheng, Z. M. 1999 On electron acceleration by intense laser pulses in the presence of a stochastic field. *Phys. Plasmas* **6**, 641–644. (doi:10.1063/1.873347)

Modena, A. *et al.* 1995 Electron acceleration from the breaking of relativistic plasma waves. *Nature* **377**, 606–608. (doi:10.1038/377606a0)

Najmudin, Z., Krushelnick, K., Tatarakis, M., Clark, E. L., Danson, C. N., Malka, V., Neely, D., Santala, M. I. K. & Dangor, A. E. 2003 The effect of high intensity laser propagation instabilities on channel formation in underdense plasmas. *Phys. Plasmas* **10**, 438–442. (doi:10.1063/1.1534585)

Nakajima, K. *et al.* 1995 Observation of ultra-high gradient electron acceleration by a self-modulated intense short laser pulse. *Phys. Rev. Lett.* **74**, 4428–4431. (doi:10.1103/PhysRevLett.74.4428)

Perry, M. D. & Mourou, G. 1994 Terawatt to petawatt subpicosecond lasers. *Science* **264**, 917–924.

Pukhov, A. 2003 Strong field interaction of laser radiation. *Rep. Prog. Phys.* **66**, 47–101. (doi:10.1088/0034-4885/66/1/202)

Pukhov, A., Sheng, Z. M. & Meyer-ter-Vehn, J. 1999 Particle acceleration in relativistic laser channels. *Phys. Plasmas* **6**, 2847–2854. (doi:10.1063/1.873242)

Santala, M. I. K., Najmudin, Z., Krushelnick, K., Clark, E. L., Dangor, A. E., Malka, V., Faure, J., Allott, R. & Clarke, R. J. 2001 Observation of a hot high-current electron beam from a self-modulated laser wakefield accelerator. *Phys. Rev. Lett.* **86**, 1227–1230. (doi:10.1103/PhysRevLett.86.1227)

Sprangle, P., Esarey, E., Ting, A. & Joyce, G. 1988 Laser wakefield acceleration and relativistic optical guiding. *Appl. Phys. Lett.* **53**, 2146–2148. (doi:10.1063/1.100300)

Tajima, T. & Dawson, J. M. 1979 Laser electron accelerator. *Phys. Rev. Lett.* **43**, 267–270. (doi:10.1103/PhysRevLett.43.267)

Tatarakis, M., Watts, I., Beg, F. N., Clark, E. L., Dangor, A. E., Haines, M. G., Norreys, P. A., Zepf, M. & Krushelnick, K. 2002 Measuring huge magnetic fields. *Nature* **415**, 280. (doi:10.1038/415280a)

Ting, A. *et al.* 1997 Plasma wakefield generation and electron acceleration in a self-modulated laser wakefield accelerator experiment. *Phys. Plasmas* **4**, 1889–1899. (doi:10.1063/1.872332)

Umstadter, D., Chen, S. Y., Maksimchuk, A., Mourou, G. & Wagner, R. 1996 Nonlinear optics in relativistic plasmas and laser wake field acceleration of electrons. *Science* **273**, 472–475.